Geochemistry Geophysics Geosystems G3
AN ELECTRONIC JOURNAL OF THE EARTH SCIENCES
Published by AGU and the Geochemical Society

Article
Volume 10, Number 2
3 February 2009
Q02002, doi:10.1029/2008GC002315
ISSN: 1525-2027

Click Here for Full Article

Volcanic inflation measured in the caldera of Axial Seamount: Implications for magma supply and future eruptions

Scott L. Nooner
Lamont-Doherty Earth Observatory of Columbia University, Palisades, New York 10964, USA (snooner@ldeo.columbia.edu)

William W. Chadwick Jr.
Cooperative Institute for Marine Resources Studies, Oregon State University and NOAA, 2115 SE OSU Drive, Newport, Oregon 97365, USA (William.W.Chadwick@noaa.gov)

[1] Since 2000, ambient seawater pressure has been precisely measured at five seafloor benchmarks inside the summit caldera at Axial Seamount to monitor volcanic inflation, using a remotely operated vehicle to deploy a mobile pressure recorder (MPR) in campaign-style surveys. Additionally, seawater pressure has been measured at the caldera center with multiyear deployments of continuously recording bottom pressure recorders (BPRs). These pressure data (converted to depth) are currently the only measurements of volcanic inflation at a submarine volcano. We show new data spanning 2004 to 2007 documenting steady inflation of 12.7 ± 0.4 cm/a at the caldera center. The spatial pattern of uplift is consistent with magma storage in a shallow reservoir underlying the caldera at a depth of ~3.5 km, and the current uplift rate implies that magma is being supplied to the volcano at a rate of $\sim 7.5 \times 10^6$ m^3/a. However, the supply rate immediately after the last eruption in 1998 was significantly higher, and the temporal pattern of uplift at Axial caldera appears to be governed by at least two processes occurring at very different time scales. We interpret the high uplift rates immediately following the 1998 eruption as either due to influx from one or more small satellite magma bodies or as the result of viscoelastic relaxation and/or poroelastic behavior of the crust surrounding the shallow magma chamber, and we present a numerical model which supports the latter interpretation. In contrast, we interpret the current lower uplift rate as due to a steady longterm magma supply from the mantle. This two component uplift pattern has not been observed on land volcanoes, suggesting that magma supply/storage processes beneath this ridge axis volcano differ from volcanoes on land (including Iceland). To reconstruct the uplift history at Axial, we fit the combined MPR and BPR data to two possible uplift scenarios, with which we forecast that the next eruption at Axial is likely to occur by about 2020, when most of the ~3 m of deflation that occurred during the 1998 eruption will have been recovered.

Components: 9166 words, 8 figures, 2 tables.

Keywords: Juan de Fuca ridge; submarine volcanism; viscoelesticity; poroelasticity; magma chamber dynamics; marine geodesy.

Copyright 2009 by the American Geophysical Union

Index Terms: 3075 Marine Geology and Geophysics: Submarine tectonics and volcanism; 8416 Volcanology: Mid-oceanic ridge processes (1032, 3614); 1207 Geodesy and Gravity: Transient deformation (6924, 7230, 7240).

Received 8 September 2008; **Revised** 10 November 2008; **Accepted** 16 December 2008; **Published** 3 February 2009.

Nooner, S. L., and W. W. Chadwick Jr. (2009), Volcanic inflation measured in the caldera of Axial Seamount: Implications for magma supply and future eruptions, *Geochem. Geophys. Geosyst.*, *10*, Q02002, doi:10.1029/2008GC002315.

1. Introduction

[2] Axial Seamount is located about 480 km west of the Oregon coast (Figure 1) at the intersection of the Cobb hot spot and the Juan de Fuca Ridge and is the most active volcanic site along the ridge [*Chadwick et al.*, 2005]. It is the locus of ocean spreading at a rate of 5–6 cm/a for about 100 km of the ridge and overlaps with the Coaxial segment to the north and the Vance segment to the south. It is also the site of the NeMO (New Millennium Observatory) seafloor observatory [*Embley and Baker*, 1999] (see also http://www.pmel.noaa.gov/vents/nemo/) and is part of a regional cabled observatory planned in the NE Pacific http://www.ooi.washington.edu/).

[3] The volcano has a 3 × 8 km horseshoeshaped summit caldera with rift zones extending ~50 km to the north and south. Caldera walls rise about 100 m above the caldera floor, which lies at a depth of about 1500 m. A summit magma chamber was imaged by *West et al.* [2001] about 3 km below the seafloor. All of the geodetic observations to date [*Chadwick et al.*, 2006b], including the subsidence of the caldera center during the 1998 eruption [*Fox*, 1999], indicate that there is a deformation source about 3.5 km beneath the center of the caldera. This suggests that all magma supplied to Axial first enters the summit magma reservoir, remains there for some time, and is then dispersed via dike injections and eruptions. Petrology of the erupted lavas at Axial supports this view [*Chadwick et al.*, 2005] and suggests mixing between hot spot and midocean ridge (MORB) basalts. The proportion of MORB in the magma increases with distance from Axial [*Chadwick et al.*, 2005]. Crustal residence time of melt in the system has been estimated to be a few hundred to a few thousand years [*West et al.*, 2001]. The underlying magma chamber also drives extensive hydrothermal venting within the caldera [*Butterfield et al.*, 1990].

[4] This paper investigates vertical deformation of the volcano during and after an eruption in 1998 using two complimentary types of measurements that use seawater pressure to infer seafloor depth. The first type of measurement is from continuously recording pressure loggers called bottom pressure recorders (BPRs). From 1987 to 1998, BPRs were deployed each year within the summit caldera at Axial to monitor vertical deformation of the seafloor. In 1998, a major dike intrusion and eruption occurred [*Dziak and Fox*, 1999b; *Embley et al.*, 1999] during which a BPR at the caldera center (VSM1, Figure 1) subsided by 3.2 m (Figure 2a), and a BPR 3 km southeast (VSM2, Figure 1) subsided by 1.4 m [*Fox*, 1999; *Fox et al.*, 2001]. This deflation was followed immediately by rapid reinflation of ~50 cm recorded on VSM1 over the next 6 months (Figure 2b) until the instrument was recovered [*Chadwick et al.*, 2006b]. There was a break in the BPR measurements at the caldera center from August 1998 until July 2000, but measurements have continued uninterrupted since then.

[5] BPRs are very useful for measuring sudden deformation events, but gradual deformation that occurs over months to years is difficult to distinguish from inherent instrument drift of uncertain rate. Therefore, a second and complimentary method was developed to measure long-term inflation by using a mobile pressure recorder (MPR) connected to a remotely operated vehicle (ROV). During each survey (typically once per year) the MPR is deployed sequentially onto an array of seafloor benchmarks to make campaign-style pressure measurements [*Chadwick et al.*, 2006b; *Stenvold et al.*, 2006]. The relative depths of the benchmarks are determined over a short period of time (hours to days) with the instrument drift constrained by making multiple measurements at each benchmark. These differential measurements began in 2000 and have been repeated every 1–2 years to track the movement of four stations inside the caldera relative to a fifth station ~10 km south of the caldera center that is assumed to be stable (Figure 1).

[6] Using both BPR and MPR data, *Chadwick et al.* [2006b] showed that from 1998 to 2004 Axial Seamount had reinflated since its last eruption;

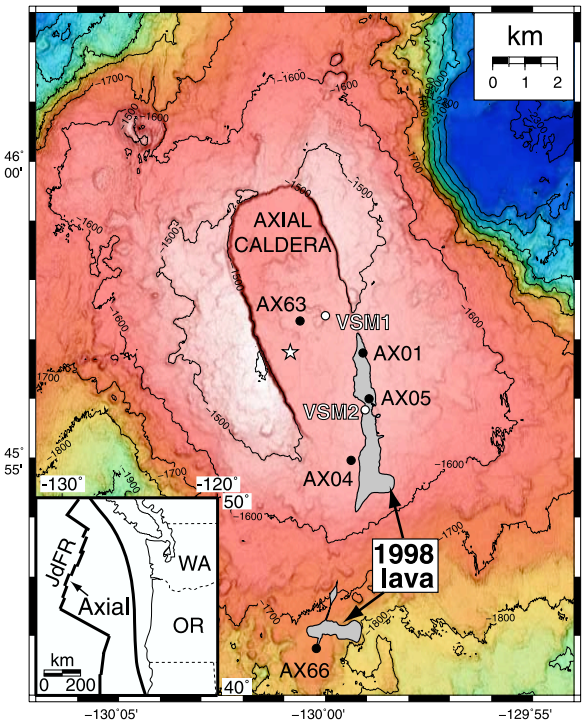

Figure 1. Map showing Axial Seamount with its summit caldera. The locations of the MPR benchmarks are shown as black dots and the location of the BPR instruments discussed in the text are shown as white dots. The best fitting Mogi inflation source for the MPR data is indicated by the white star. The 1998 lava flow is outlined in black and depth contours are shown with a 100 m spacing.

here, we present additional MPR and BPR data from 2004 to 2007 that show inflation is continuing. Furthermore, the lower uncertainty in the most recent MPR measurements reveals that the rate of uplift has changed with time. The character of this change suggests that there are two simultaneous deformation mechanisms operating at Axial volcano, a transient short-term mechanism and a steady long-term mechanism. We attribute the steady, lowrate, long-term inflation to magma recharge from a deep source, consistent with observations from many volcanoes on land. The higher-rate, shortduration inflation immediately following the 1998 eruption, however, may be uniquely measurable at submarine volcanoes. We develop two conceptual models to explain this observation, both of which suggest that a significant amount of magma recharge comes from local sources within a few months after an eruption.

[7] We also combine the MPR and BPR data to reconstruct the history of uplift at Axial across a gap in the geodetic observations. We use this history to infer rates of magma supply and total uplift of the caldera, with implications for the recurrence interval between eruptions.

2. Methods and Results

2.1. Mobile Pressure Recorder Data

[8] MPR surveys were carried out using the Canadian ROV *ROPOS* on board the R/V *Thomas Thompson* in 2006 and the ROV *Jason* on board the R/V *Atlantis* in 2007. BPR data was recorded at the caldera center from 2004 to 2007 and was used to correct the MPR data for ocean tides. The linear

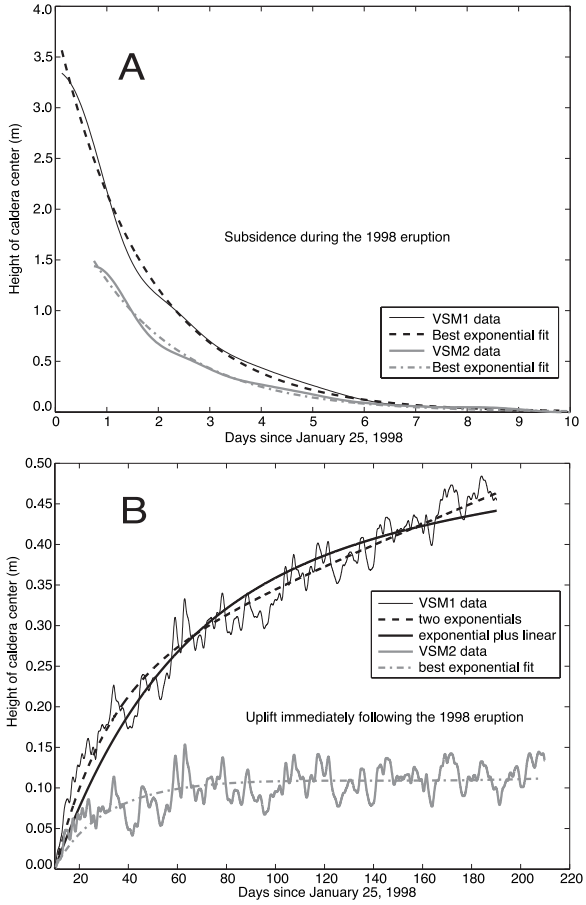

Figure 2. (a) Coeruption subsidence measured in 1998 by the VSM1 (black) and VSM2 (gray) BPRs (Figure 1) with the best fitting exponential curves. (b) Rapid posteruption reinflation from the VSM1 (black line) and VSM2 (gray line) BPRs with fit scenarios discussed in the text. Shown for VSM1 are an exponential plus a linear term (thick solid line, scenario 1) and the sum of two exponentials (thick dashed line, scenario 2). Shown for VSM2 is the best fitting exponential (gray dash dot line). Time is given in days since 25 January 2008, which marks the beginning of the eruption.

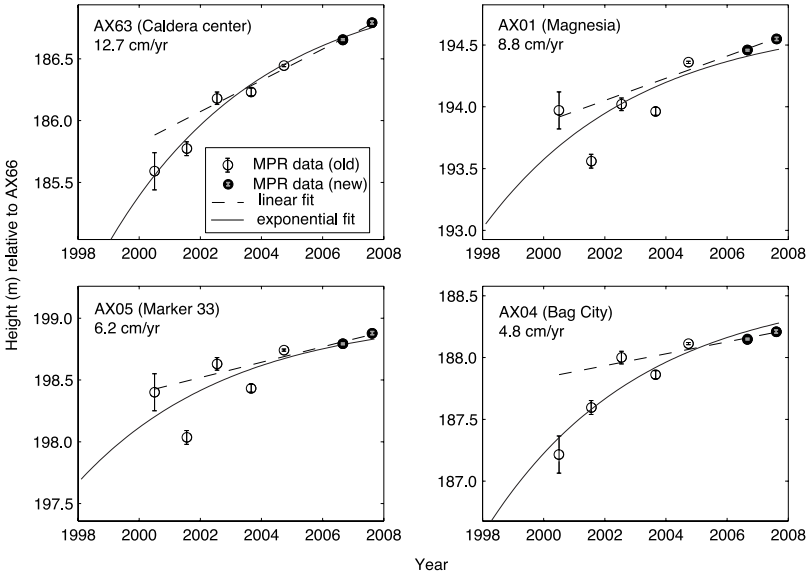

Figure 3. MPR benchmark heights relative to the reference, AX66, are shown as a function of time for each station inside the caldera (see Figure 1). The MPR data at each benchmark are fit to a line using a weighted least squares (dashed) and to an exponential (solid) using an iterative inversion. For the exponential fits, the time constant used was the value that best fit the data at AX63 (caldera center). The value of the linear uplift rate is given at each benchmark. The new data presented in this study are shown as solid black circles.

drift of the MPR instrument was determined each year from repeated measurements on each benchmark. In both 2006 and 2007, AX63 and AX66 were measured twice; the remaining three benchmarks were measured three times each. After correcting for ocean tides and linear instrument drift, the repeatability of the new MPR measurements from 2006 and 2007 were 0.6 cm and 1.1 cm, respectively (Figure 3), similar to the 0.9 cm repeatability achieved in 2004 by *Chadwick et al.* [2006b]. The data processing methods are described in more detail by *Chadwick et al.* [2006b] and *Nooner* [2005].

[9] The complete time series of MPR measurements at Axial Seamount is shown in Figure 3, with the elevation of the four benchmarks in the caldera shown relative to benchmark AX66, which is treated as fixed. All four stations are uplifting with rates that decrease with distance from the caldera center (Table 1). During the first few years of MPR measurements at Axial Seamount, the uncertainties were relatively high and are difficult to quantify. Uncertainties have decreased by nearly two orders of magnitude from these early measurements as we have developed an understanding of the sources of error and better techniques for quantifying uncertainty [*Chadwick et al.*, 2006b; *Nooner*, 2005]. The large uncertainty in the early MPR measurements poses problems for data analysis. The simultaneous BPR measurements, however, demonstrate that the depth changes inferred from MPR measurements between years can be interpreted in terms of a slowly varying uplift rate rather than the result of intermittent or abrupt motions (Figure 4).

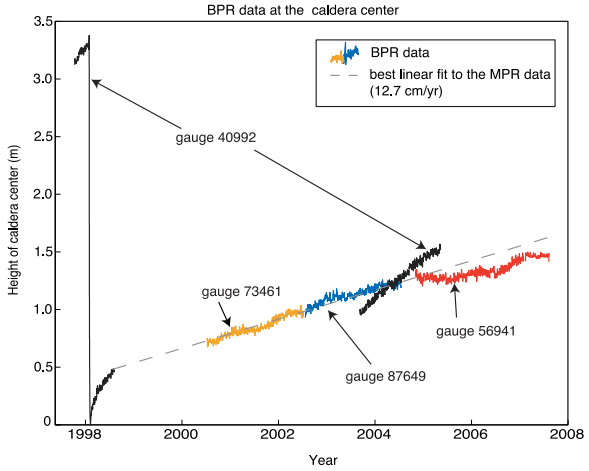

Figure 4. BPR data recorded since 1997 at the caldera center are shown with arbitrary vertical offsets to make them align. Different colors indicate different BPR instruments. The apparent inflation rate for most of the instruments is close to the 12.7 cm/a from the MPR data (Figure 3a) for most of the records. Although long-term drift rates are different from one BPR to the next, it is clear that no sudden depth changes have occurred. The BPR with the high apparent uplift rate is the same gauge that was used in VSM1. See text for discussion.

Table 1. Parameters for Linear and Exponential Fits to the Data

		Weighted Linear Fit		Best Single Exponential Fit	
Site and Data Set	Time	Inflation Rate (cm/a)	Standard Deviation of Residuals[a] (cm)	A, τ	Standard Deviation of Residuals[a] (cm)
VSM1-BPR	eruption	N/A	N/A	350 cm, 1.74 days	5.8
VSM1-BPR	posteruption	N/A	N/A	50 cm, 59 days	2.7
VSM2-BPR	eruption	N/A	N/A	149 cm, 1.82 days	2.8 cm
VSM2-BPR	posteruption	N/A	N/A	11 cm, 21.9 days	1.9 cm
AX63-MPR	2000–2007	12.7 ± 0.4	13.6	255 cm, 5 years	6.2
AX01-MPR	2000–2007	8.8 ± 0.4	18.7	170 cm, 5[b] years	25.1
AX05-MPR	2000–2007	6.2 ± 0.4	18.8	130 cm, 5[b] years	27.6
AX64-MPR	2000–2007	4.8 ± 0.4	25.5	200 cm, 5[b] years	16.0

[a] The standard deviation of residuals is a measure of how well the model fits the data.
[b] The time constant was forced to equal the best fit for the MPR data at the caldera center.

[10] The MPR data at each benchmark can be fit with a linear uplift rate using weighted least squares (Figure 3); for example, the best fitting linear uplift rate at the caldera center (AX63) is 12.7 ± 0.4 cm/a. The spatial pattern of the best fitting linear deformation rates are consistent with a point source of inflation in an elastic halfspace [*Mogi*, 1958] located 1 km south of the caldera center at a depth of 3.5 km (Figure 5). This is in general agreement with model source locations from previous geodetic work at Axial [*Chadwick et al.*, 1999; *Chadwick et al.*, 2006b; *Fox et al.*, 2001] and with the depth of low velocity or melt zones that were imaged seismically below the caldera [*Kent et al.*, 2003; *West et al.*, 2001]. On the basis of the point source fit to the data, AX66 should be uplifting by up to 0.5 cm/a rather than being fixed. However, this is less than the uncertainty of the measurements each year, so it has little effect on our results.

[11] Although a linear fit to the MPR data gives reasonable results, the uplift rates appear to have decreased with time at some of the benchmarks (Figure 3). This is particularly evident at the caldera center (AX63) where the signal-to-noise ratio is highest and the uplift appears to be quasi-exponential. Therefore, exponential curves with a decreasing uplift rate over time have also been fit to the MPR data. However, given the scatter and uncertainty in the early MPR data points, it is hard to determine unambiguously whether linear or exponential curves better describe the pattern of inflation. Nevertheless, it is clear that immediately after the coeruption deflation of 3.2 m (Figure 2a), the rate of reinflation recorded by the VSM1 BPR was initially much higher than the current rate of inflation and decreased quasi-exponentially over the following 6 months (Figure 2b). Also, the coeruption deflation followed an exponential curve (Figure 2a), showing that nonlinear inflation/deflation patterns are clearly important at Axial.

2.2. Bottom Pressure Recorder Data

[12] Figure 4 shows all of the BPR data that has been recovered from the caldera center since 1998. Each BPR data set is offset in absolute depth from others because the instruments were at slightly different locations and depths from deployment to deployment. Nevertheless, the BPR data still provide valuable constraints on the rate and continuity of deformation. For Figure 4, the different BPR data sets have been vertically offset to fall approximately on the 12.7 cm/a line that was obtained from a linear fit to the MPR data at the caldera center (discussed in section 2.1, Figure 3). No changes have been made to the measured BPR uplift rates. The BPR data from the caldera center

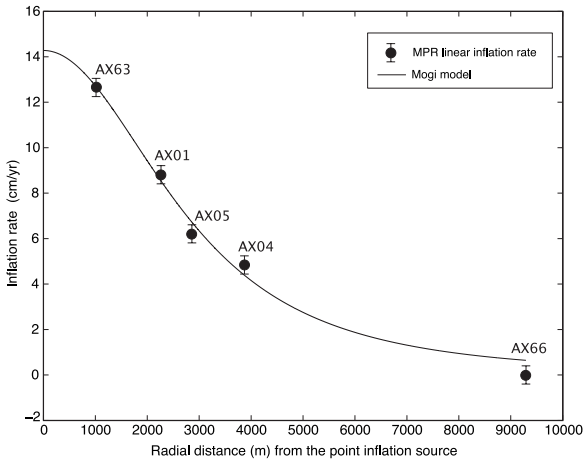

Figure 5. The best fitting linear inflation rates from the MPR measurements fit a Mogi point source model located about 1 km SSW of the caldera center (Figure 1) at a depth of 3.5 km.

have yielded essentially linear apparent inflation rates that typically range from 11 to 13 cm/a (Figure 4) since 2000, with 11 cm/a being the most recent data from gauge 56941. The outlier is an apparent 34 cm/a recorded on the same pressure gauge [40992] that was also in the VSM1 BPR. The observed pressure changes are a combination of motion of the seafloor and instrument drift. The actual BPR instrument drift cannot be constrained independently of the MPR measurements and may be up to 23 cm/a at Axial [*Chadwick et al.*, 2006b]. Comparing the BPR data to the best linear fit of the MPR data at the caldera center allows us to determine the average BPR drift rates in recent years when the MPR measurements have low uncertainty (2003–2007). Given how well the BPR data fit the 12.7 cm/a trend from the MPR measurements, there appears to be very little, if any, long-term drift in most of the BPR gauges. Only gauge 40992 shows a clear drift signal, with an amplitude of about 21 cm/a, consistent with what is seen in the 1997–1998 VSM1 data and during three previous deployments of this gauge at Axial seamount from 1992 to 1996 (W. W. Chadwick and C. G. Fox, unpublished data, 1996). These data suggest that not only are most gauges much better than expected and are consistent from deployment to deployment but also that the uplift at Axial has been nearly linear since 2000 and supports the interpretation that the apparent noise in the early MPR measurements is primarily due to measurement error. The BPR data also show that there have been no episodic events or sudden depth changes from 2000 to 2007.

3. Quantifying Deformation at Axial Seamount

3.1. Coeruption Subsidence

[13] Volcanic eruptions often occur in the form of a diking event, especially in regions of tension like a spreading center. Dikes appear to originate from a central magma chamber and propagate at a rate of 1–3 km/h [*Dziak and Fox*, 1999b]. Numerical models of dike ascent in partially molten rock [*Rubin*, 1998] indicate that large dikes in the crust can only tap magma from regions with large amounts of concentrated melt, rather than from regions of partial melt. This is because porous flow from a partial melt region cannot provide magma sufficiently rapidly to feed a dike that is more than a few millimeters wide. Therefore, an eruption usually leads to a large pressure change in the magma chamber as fluid rapidly moves out into the dike. This pressure decrease in the magma chamber leads to subsidence of the overlying elastic crust.

[14] Subsidence during eruptions can be modeled as the feeding of a dike by flow of magma from the magma chamber through a cylindrical pipe in an elastic material. The removal of magma during eruptions decreases the pressure within the shallow magma chamber, which causes propagation of the dike to slow exponentially [*Dvorak and Dzurisin*, 1997]:

$$Q = Q_0 e^{-t/\tau} \tag{1}$$

where Q_0 is the initial magma flux at time $t = 0$. The time constant, τ, is given by

$$\tau = \frac{8\eta}{\pi} \frac{\Delta V}{f r^4} \left(\frac{l}{\Delta P} \right) \tag{2}$$

for a Poiseuille flow where η is the viscosity of the magma, ΔV is the volume change, f is the friction loss factor, r is the radius of the pipe, and $\Delta P/l$ is the pressure gradient between the two reservoirs. The rate of flow (and subsidence) depends on the pressure difference between the summit magma chamber and an intrusive dike and decreases exponentially with time until the driving pressure is too low. Coeruptive subsidence is generally observed to occur with a timescale on the order of a few days. This type of behavior has been observed at Kilauea and Mauna Loa volcanoes, Hawaii [*Dvorak and Okamura*, 1987; *Tilling and Dvorak*, 1993]; Krafla, Iceland [*Björnsson*, 1985; *Sturkell et al.*, 2006; *Sturkell et al.*, 2003; *Tryggvason*, 1980]; Westdahl volcano, Alaska [*Lu et al.*, 2003]; Sierra Negra, Galapagos [*Geist et al.*, 2008]; and now at Axial Seamount (Figure 2a).

[15] *Fox* [1999] noted that subsidence during the 1998 eruption of Axial appeared to be quasi-exponential. Here we quantify the fit of the VSM1 data to an exponential curve, $z = Ae^{-t/\tau}$, with a time constant, τ, of 1.74 days and amplitude, A, of 3.5 m (Figure 2a and Table 1). The VSM2 data fit an exponential with τ = 1.82 days and A = 1.5 m (Figure 2a and Table 1). The time constants of exponentially decaying subsidence observed at other volcanoes during eruptions vary, ranging from 0.25 days to 21 days at Kilauea and Mauna Loa [*Dvorak and Okamura*, 1987], but are close to 1.5 days at Krafla [*Tryggvason*, 1980] and Westdahl [*Lu et al.*, 2003]. Therefore, at least for the 1998 diking event, the coeruptive subsidence of Axial closely resembles that of some basaltic volcanoes on land.

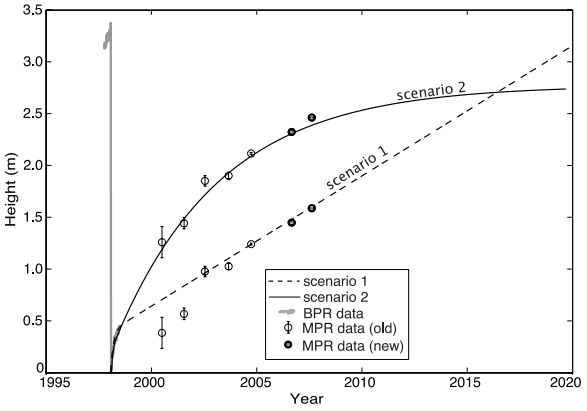

Figure 6. Two scenarios for the pattern of inflation at the caldera center since the 1998, eruption, combining the coeruption BPR data with the posteruption MPR measurements (discussed in the text). In both scenario 1 (a short time constant exponential plus a linear term) and scenario 2 (a sum of two exponentials with different time constants), the volcano will have reinflated and presumably ready to erupt by 2020. The new data presented in this study are shown as solid black circles.

3.2. Posteruption Uplift

[16] Linking the BPR and the MPR data across the data gap that occurred from August 1998 to July 2000 is a key to understanding the behavior and total reinflation of the volcano since its 1998 eruption. However, this is complicated by the fact that there is an unknown vertical offset between the two data sets. There are also two sources of error in combining the BPR and MPR data sets at the caldera center: (1) instrumental drift in the VSM1 BPR data and (2) the VSM1 BPR was located 800 m from the AX63 MPR benchmark (caldera center). As noted in section 2.2, gauge 40992 used in the VSM1 BPR showed a drift of about 21 cm/a and therefore its record includes 10–11 cm of drift-induced apparent inflation in the 6-month posteruption BPR data. The other source of error is that VSM1 and AX63 were not collocated. The best fitting Mogi model of the inflationary source (Figure 5) indicates that the uplift at the location of VSM1 was ~20% less than the uplift at benchmark AX63 (caldera center). This means that VSM1 uplifted about 10 cm less than the uplift predicted at the caldera center over this 6-month period. These two sources of error are about the same magnitude and in opposite directions. For simplicity, we will assume in the rest of the paper that they exactly cancel and we treat the VSM1 data as though it were obtained at the caldera center and not affected by sensor drift.

[17] At Axial, as soon as the 1998 diking event ended, rapid reinflation appeared in both the VSM1 and the VSM2 BPR data but at a rate that decayed quasi-exponentially over a period of days to months. Fitting the VSM1 data with the exponential curve $z = A(1-e^{-t/\tau})$ gives an amplitude, A, of 0.5 m and a time constant, τ, of 59 days (Figure 2b; Table 1). Fitting the first 200 days of VSM2 reinflation data gives A = 0.11 m and τ = 22 days (Figure 2b; Table 1).

[18] The MPR data collection started in 2000, more than 2 years after the 1998 diking event. In section 2.1, we fit the MPR data with both a linear curve and an exponential curve at each site, $z = A(1-e^{-t/\tau})$. The best fitting exponential curve for the caldera center has A = 2.55 m and τ = 5 years. In fitting the exponential curves, the start time was chosen to coincide with the beginning of reinflation observed on VSM1 (3 February 1998 at 1900 UT). Since the MPR measurements give relative depths, the depth offset from zero is not known. Therefore we constrain the best fitting curve to have zero depth offset at time t = 0, shifting the MPR data up or down to meet this constraint. The time constants for the exponential curves at the other benchmarks are forced to equal the time constant determined at the caldera center (AX63) since this is the site with the best signal-to-noise ratio. Compared to a linear fit, exponential curves reduce the scatter of the residuals at stations AX63 and at AX04 but not at AX01 and AX05 (Figure 3 and Table 1). This is probably due to the large uncertainty in the measurements from 2000 to 2003, as discussed above.

[19] To reconstruct the history of uplift since the 1998 eruption the MPR and BPR data sets must be linked across the data gap. The exponential fit to the VSM1 BPR reinflation data demonstrates that the uplift rate rapidly decreased over a period of 6 months. However, when geodetic measurements resumed in 2000, the uplift trend was slow and steady in both the MPR and the BPR data and could be interpreted as either linear or exponential. Therefore, two different scenarios are constructed for the post-1998 reinflation at the caldera center, each a combination of two curves. In the first scenario (Figure 6), the posteruption BPR data and the MPR data are fit together with an exponential curve plus a linear term, $z = A(1-e^{-t/\tau}) + mt$. The slope of the linear term was taken from the MPR data and held fixed at m = 12.7 cm/a. The best fit exponential has τ = 48 days and A = 0.39 m. The combined curve reduces the scatter of the BPR data residuals compared to just a single exponential

Table 2. Fit Parameters for Linking the BPR and MPR Data Sets at the Caldera Center

Parameter	Value
Exponential Plus Linear	
A, τ	39 cm, 48 days
Linear rate	12.7[a] cm/a
Standard deviation of residuals[b]	2.6 cm
Two Exponentials	
A_1, τ_1	23 cm, 21 days
A_2, τ_2	255 cm, 5 years[c]
Standard deviation of residuals[b]	2.0 cm

[a] The linear rate was forced to equal the best fit to the MPR data at the caldera center.
[b] The standard deviation of residuals was calculated for the VSM1 BPR data. This is a measure of how well the model fits the data.
[c] The amplitude and time constant were forced to equal the best fit for the MPR data at the caldera center.

fit (Tables 1 and 2). This scenario results in a net uplift of 1.6 m at the caldera center from the 1998 eruption to August 2007, corresponding to a total volume change of 8.89×10^7 m^3 within the crust, assuming a Mogi source.

[20] Another way to link the posteruptive MPR and BPR results (scenario 2 in Figure 6) is to fit both data sets with a function that is the sum of two exponentials. First, one exponential term was determined by the MPR data (AX63) and held fixed with $\tau_2 = 5$ years and $A_2 = 2.55$ m, then the BPR data were fit with the equation $z = i(1-e^{-t/\tau}) + A_2(1 - e^{-t/\tau_2})$. The resulting short time constant, small amplitude exponential has $\tau = 20$ days and $A = 0.23$ m. Again, this reduces the scatter of BPR residuals (Table 2). For comparison, the exponential time constant during inflation at Westdahl volcano, Alaska, was found to be about 6 years [*Lu et al.*, 2003], similar to what we see in the MPR data at the caldera center. At Kilauea volcano, Hawaii, which has a much larger magma supply than Axial, the time constant during multiple reinflation events from February to September 1983 was found to be about 40 days, similar to what we see in the BPR data right after eruption [*Dvorak and Okamura*, 1987]. The amount of net uplift predicted by this scenario at the caldera center as of August 2007 is 2.5 m, corresponding to a volume change of 14.8×10^7 m^3 within the crust, again assuming a Mogi source.

[21] Thus, we can interpret the overall pattern of inflation from 1998 to 2007 using either of these two scenarios (Figures 2 and 6): (1) a short time constant exponentially decaying uplift superimposed on a linear inflation or (2) a short time constant exponentially decaying uplift superimposed on a long time constant exponentially decaying inflation. In both scenarios, the inflation decays rapidly over the first 6 months then becomes dominated by either a longer exponential time constant or a slower linear inflation rate. The large uncertainty in the first few years of MPR measurements does not allow us to conclusively differentiate between a long-term linear or exponential inflation, but the predictions from each scenario are rapidly diverging (Figure 6); by 2010, the predictions will have diverged by ~20 cm and by ~70 cm in 2015. Thus, with continued monitoring we should easily be able to distinguish between linear and exponential inflation within the next 5 years.

4. Physical Deformation Models for Axial Seamount

[22] As discussed above, fitting the combined BPR and MPR inflation data set requires a low amplitude exponential with a short time constant superimposed upon either a longterm linear rate or a larger amplitude exponential with a longer time constant. This implies that there are two distinct underlying processes causing the inflation. Next, we discuss two conceptual models that might explain this distinctive pattern in the observed deformation. In both models we believe that the long-term lower rate of inflation at Axial reflects the continuous magma supply rate from the mantle, indicating that there is a hydraulic connection between the shallow crustal magma chamber and the deeper melt source region. Consistent with an inferred deep magma source at Axial Seamount, *West et al.* [2001] observed a low velocity zone extending below the shallow magma chamber down to more than 6 km below the seafloor with seismic tomography.

[23] Hydraulic connection between shallow magma chambers and a deeper source has also been inferred from geodetic measurements of volcanoes on land. *Dvorak and Okamura* [1987] modeled posteruption inflation at Kilauea and Mauna Loa, Hawaii, as flow from a deep source at a constant pressure into a shallow magma chamber through a cylindrical pipe. This connection has also been made at Grimsvotn volcano in Iceland [*Sturkell et al.*, 2003] and Westdhal volcano in Alaska [*Lu et al.*, 2003]. An exponentially decreasing uplift rate is expected from this simple hydraulic model with a timescale on the order of several years. A linear inflation rate would imply that the pressure difference between the shallow reservoir and the deep source remains constant.

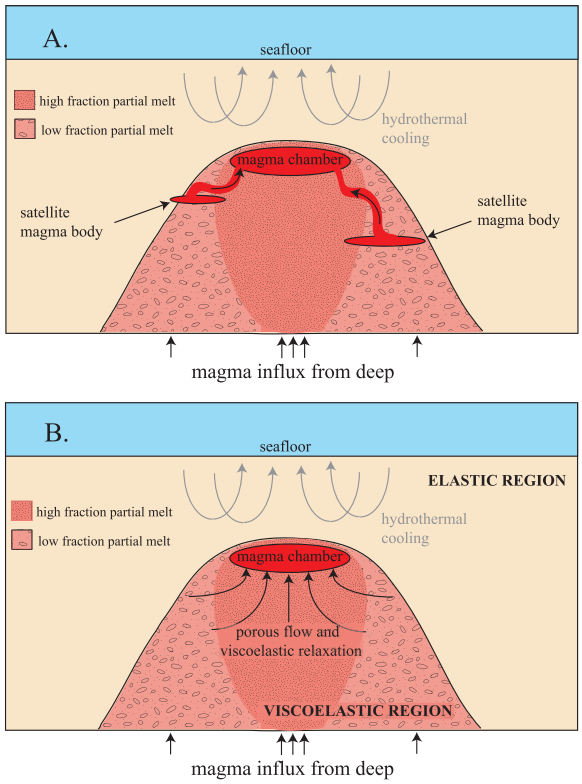

Figure 7. Two conceptual magma chamber models within the upper crust at Axial Seamount that could explain the observed rapid reinflation after the 1998 eruption. (a) Conceptual model 1 consists of rapid recharge of the magma chamber from local satellite magma bodies. (b) Conceptual model 2 consists of viscoelastic relaxation of the partial melt region plus porous flow of melt from the partial melt into the magma chamber. Both models include lower-rate, steady magma recharge from depth.

[24] The most intriguing part of the inflation signal at Axial is the short-lived transient deformation observed immediately after the 1998 eruption that is superimposed upon the slower steady magma recharge signal. This compound pattern of volcanic inflation has not previously been described, suggesting that it may be related to the geologic setting of Axial Seamount. The two conceptual models discussed below describe two mechanisms that could be responsible for the observed short-term inflation.

4.1. First Conceptual Model

[25] In the first model, the initial rapid inflation after the 1998 eruption is caused by the flow of magma from one or more nearby smaller satellite magma bodies through narrow conduits into the main summit magma chamber (Figure 7a). This could occur because the connected reservoirs were initially at the same (high) internal pressure, but the pressure in the larger chamber was suddenly reduced during the eruption, causing rapid flux of magma from the satellite magma bodies. If viewed in terms of pipe flow, the conduit length between these shallow reservoirs, l in equation (2), is small, making τ short. At the same time, magma is also being supplied to the main magma chamber from a deeper source (i.e., with l much longer), superimposing slow steady inflation. Some surface subsidence over these (hypothetical) satellite magma bodies would be expected to occur as magma flows out and into the main reservoir. There is no evidence for such subsidence, but since there were only two BPRs recording inside the caldera immediately after the 1998 eruption (VSM1 and VSM2, Figure 1), there is not enough geodetic data to confirm or refute this model. The possibility of shallow satellite reservoirs has been suggested by preliminary analysis of multichannel seismic (MCS) data from *Kent et al.* [2003], which shows that there may be a shallow melt bodies to the southeast of the caldera. *Sohn et al.* [2004] observed elevated rates of seismicity on the southeast edge of the caldera for about 60 days following the 1998 eruption, which they attribute to thermal contraction related to the 1998 eruption. Otherwise all the existing geodetic data at Axial consistently point to a single inflationary/deflationary source, but the possibility of small satellite magma bodies on the periphery of the caldera cannot be ruled out.

4.2. Second Conceptual Model

[26] The second conceptual model for the short-term transient inflation at Axial includes a short-lived viscoelastic and poroelastic response phase immediately after the 1998 eruption. In this model, a sill-like magma reservoir is overlain by an elastic layer and embedded in a hot viscoelastic region containing a small percentage of partial melt (Figure 7b). This model geometry is consistent with thermal models [*Hodge*, 1974] and seismic studies of fast spreading midocean ridges [*Sinton and Detrick*, 1992; *Toomey et al.*, 1990; *Vera et al.*, 1990; *West et al.*, 2001; *Wilcock et al.*, 1992].

[27] In our conceptual model, an eruption causes a rapid pressure drop within the magma chamber as magma is withdrawn to feed the dike, resulting in a rapid change in the surrounding stress field. The initial (elastic) response of the system is subsidence of the seafloor. The posteruption magmatic system then reequilibrates by (1) porous flow of melt from

the partial melt region into the magma chamber and (2) viscoelastic relaxation of the hot rock matrix surrounding (but mainly below) the magma chamber. The contribution of each depends on the permeability, magma viscosity, and bulk viscosity of the partial melt region. This flow of material toward and into the drained magma chamber, due to its sudden decrease in internal pressure, leads to uplift of the seafloor directly above the magma chamber.

[28] Transient deformation that may be related to viscoelastic or poroelastic relaxation has been observed at other volcanic systems in places such as Iceland, Alaska, and Long Valley caldera, California [*Foulger et al.*, 1992; *Hurwitz et al.*, 2007; *Masterlark and Lu*, 2004; *Newman et al.*, 2001; *Sigmundsson*, 2007]. Most of these studies, however, examine either long timescale (years) viscoelastic relaxation or poroelastic effects caused by shallow groundwater effects above the magma chamber or withdrawal of volatiles that are released from the magma. The model we propose for Axial is that viscoelastic relaxation along with the flow of magma from the partial melt region into the depressurized magma chamber cause the observed rapid surface deformation immediately following the eruption.

[29] *Dragoni and Magnanensi* [1989] consider analytical models of deformation caused by a spherical inflation source (magma chamber) surrounded by a viscoelastic shell (partial melt region) and embedded in an elastic space. *Newman et al.* [2001] extend this to numerical models of the same geometry in an elastic halfspace. The idealized model geometries of *Dragoni and Magnanensi* [1989] and of *Newman et al.* [2001] give insight into the behavior of viscoelastic materials but do not adequately describe the physics at Axial Seamount or at midocean ridges. After an eruption, a spherical magma chamber surrounded by a spherical shell of viscoelastic material will relax uniformly in all directions, causing transient subsidence on the surface. In contrast, at Axial we observe transient uplift. This difference is due to the differences between their models and ours; their model consists of a spherical magma chamber surrounded by a spherical viscoelastic shell, whereas ours consists of a silllike magma chamber sandwiched between elastic and viscoelastic layers (Figure 7b).

[30] Tomographic studies at Axial [*West et al.*, 2001] illustrate that the shallow magma chamber is not uniform in shape and is surrounded by hot material below and to the sides. This is reinforced by shallow MCS data that show no low velocities below the caldera of Axial to at least 1.4 km depth [*Van Heeswijk*, 1986]. Numerous other studies of midocean ridges indicate that melt is concentrated in a thin lens at the top of a large hot region of partial melt [*Sinton and Detrick*, 1992; *Toomey et al.*, 1990; *Vera et al.*, 1990; *Wilcock et al.*, 1992]. In this view, the brittle to ductile transition above the magma chamber occurs over a very short spatial scale due to cooling from hydrothermal flow (Figure 7b). Therefore, we expect that after the initial elastic subsidence, posteruption stresses would be partially relieved by viscoelastic relaxation and porous flow of melt from below and from the sides, but not from above, leading to uplift rather than subsidence over the magma chamber. A small amount of subsidence would occur some distance away from the caldera center.

[31] This behavior can be investigated with a numerical model consisting of a thin rectangular magma body embedded in a viscoelastic layer and overlain by an elastic layer (Figure 8b). The magma chamber is filled with a low viscosity viscoelastic material. Constant tractions directed inward are applied to the boundaries of the magma chamber. The results (Figure 8a) show that the initial response of the system is subsidence followed by uplift due to viscoelastic relaxation of the surrounding partial melt region. In this example model, an average viscosity of 10^{16} Pa s in the partial melt region yields a reinflation of about 12% after 6 months; this is equivalent to about 40 cm of rapid reinflation at Axial. However, careful modeling which incorporates more realistic geometries and boundary conditions, and includes poroelastic effects, is needed to do anything other than illustrate that this model is a plausible mechanism for uplift. This example model was calculated using the 3D finite element modeling code PyLith [*Aagaard et al.*, 2007; *Williams*, 2006; *Williams et al.*, 2005], freely available through the Computational Infrastructure for Geodynamics.

5. Discussion

5.1. Eruption Cycle at Axial Seamount

[32] Following the 1998 eruption, the magma supply rate at Axial (based on a Mogi model and ignoring magma compaction) decreased from 1.4×10^8 m^3/yr the first month to 3.6×10^7 m^3/a six months later. By 2002 or 2003, the supply rate had decreased further to about 7.5×10^6 m^3/a.

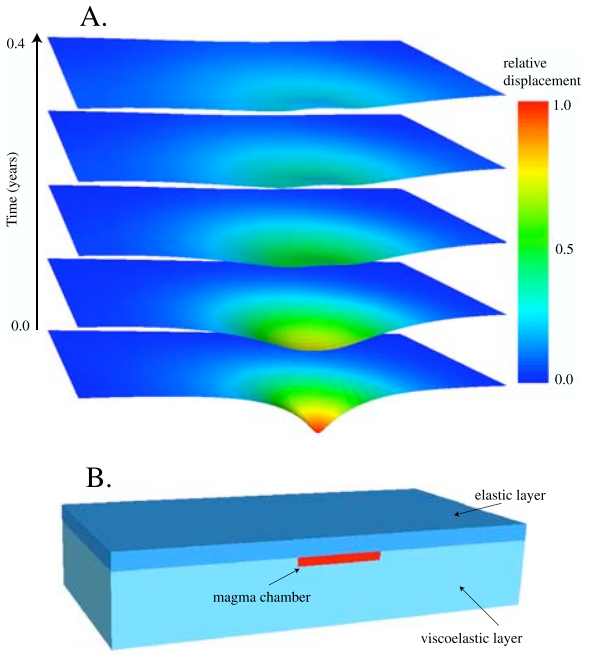

Figure 8. (a) Output of an example 3-D viscoelastic model showing seafloor deformation with time after an eruption. (b) We model an eruption event as a sudden decrease in pressure in a thin rectangular magma chamber that is overlain by an elastic material and surrounded below and to the sides by a viscoelastic material. This pressure change leads to a compaction of the magma chamber with associated subsidence of the seafloor in the first time step. Over time, relaxation of the viscoelastic material causes the seafloor to rebound above the magma chamber.

These observations can be explained by the two conceptual models presented above, in which initial rapid uplift is caused by either magma influx from a shallow satellite magma body or by local poroelastic/viscoelastic effects. These models suggest that after the eruption 7–11% of the total expected volume of magma replenishment came from shallow sources within the first 6 months, and the remainder has come from a deeper mantle source. This estimate is obtained by comparing the total expected uplift (~3 m) to the amplitudes of the best fitting short time constant exponentials (0.23 m and 0.39 m, Figure 5). These intriguing observations imply physical processes that may also occur at other submarine volcanoes and mid-ocean ridges, but Axial is currently the only one with a time series of surface deformation.

[33] The reconstructed history of uplift can also be used to make future forecasts about the eruption cycle at Axial. We hypothesize that when uplift within Axial caldera has recovered most of the ~3 m of subsidence that occurred during the 1998 eruption it will be ready to erupt again (Figure 6). If the first scenario is correct and inflation continues at the current linear rate, the magma chamber will refill to pre-1998 eruption levels by 2020. If the second scenario is correct and future inflation follows an exponential curve that is asymptotically approaching ~2.78 m of inflation, 99% of the reinflation will have taken place by 2020. On the basis of the data available at the time, *Chadwick et al.* [2006b] estimated an eruption recurrence interval at Axial of 16 years. The current longer data set suggests that the interval may be up to 22 years, assuming that eruptions recur at similar inflation levels. However, it is worth noting that the pattern of magma supply to basaltic volcanoes can change dramatically over short periods of time. This is well illustrated by recent GPS monitoring at Sierra Negra volcano, Galapagos. Inflation within Sierra Negra caldera has been following an exponentially decreasing curve since its October 2005 eruption [*Ruiz et al.*, 2007]. However, the pattern of inflation just before that eruption was completely different and was characterized by accelerating uplift [*Chadwick et al.*, 2006a], possibly due to a surge in magma supply.

5.2. Differences Between Diking at Axial Seamount and at Volcanoes on Land

[34] The behavior at Axial shows remarkable differences to hot spot/spreading regions on land. The most recent diking episode at Krafla, Iceland (1975–1984), comprised about 20 discrete events spanning 9 years. More recently, a rifting episode began in 2005 on the Afar rift [*Wright et al.*, 2006], and has already included more than 10 diking events and enhanced levels of seismicity over a several year interval [*Ebinger et al.*, 2008; *Wright et al.*, 2006]. In both Iceland and the Afar, the initial dikes were the largest and were not accompanied by any significant surface eruptions [*Tryggvason*, 1994; *Wright et al.*, 2006]. Extrusions of lava in Iceland occurred primarily in the later diking episodes [*Tryggvason*, 1994] and have so far been minor in the Afar. In contrast, in 20 years of studying Axial, only one major diking event has been observed, and there has been very little seismic activity other than in the months leading up to and including the 1998 eruption [*Dziak and Fox*, 1999a, 1999b]. This suggests that the eruption cycle at Axial is different in character than rifting events on land in that it appears to consist of single events spaced apart by 15–20 years, rather than clusters of 10–20 diking events separated by 100–

300 years. Another difference is that the temporal inflation patterns observed at Axial differ from those observed at basaltic volcanoes on land during a typical eruption cycle. For the single event that has been observed at Axial there is a rapid but short exponentially decaying inflation period followed by a more steady long-term inflation. In Iceland, for example, the short-term transient uplift signal is not seen and reinflation typically follows a single long-term exponential curve [e.g., *Sturkell et al.*, 2003].

[35] In comparison with Iceland and the Afar, the crust and lithosphere at Axial is thin and the spreading rate is high. Additionally, the magma supply rate at Axial is large enough to support a continuously supplied shallow magma reservoir [*Perfit and Chadwick*, 1998]. This relatively constant flux of hot magma flowing from the mantle to the crust could act to reduce magma crystallization in the partial melt region, thereby enhancing the connectivity of the melt surrounding the magma chamber. A pressure drop within the magma chamber would then drive porous flow from the partial melt region into the magma chamber more rapidly at Axial than on land.

[36] Additionally, the thinner and warmer lithosphere at Axial (8–11 km) [*West et al.*, 2003] may not be able to sustain the stresses that build up in the thicker lithosphere of Iceland (25–40 km) and the Afar (17–25 km), causing events at Axial to be smaller and more frequent relative to its spreading rate. This in turn could limit the size of the magma chamber by limiting the duration of magma accumulation between events. The relative pressure drop caused by an eruption would then be increased at Axial relative to land volcanoes, leading to increased viscoelastic relaxation and more rapid flow of material from local sources back into the summit reservoir.

6. Conclusions

[37] A combination of BPR and MPR data sets constrains the temporal and spatial character of deformation at Axial seamount. Coeruption subsidence can be modeled as fluid flow between the summit reservoir and an intrusive dike. Posteruption inflation, however, appears to be governed by two different processes occurring at very different timescales. Initial uplift immediately after the 1998 eruption was very rapid but decayed exponentially over the next few months, and subsequent inflation has been either linear or has been exponentially decaying at a much slower rate. The initial rapid reinflation can be explained by one of two conceptual models: (1) influx of magma into the summit magma chamber from shallow satellite magma bodies, or (2) viscoelastic relaxation plus porous flow of melt from the partial melt region that underlies the magma chamber. Results from a simple viscoelastic model are consistent with the second conceptual model, but more sophisticated numerical modeling is needed to better constrain the range of rheology and permeability that are required to explain these effects. These two conceptual models result in differing surface deformation and could be distinguished with better spatial coverage of the geodetic data. Influx from a satellite magma body would cause focused subsidence over that body and uplift over the refilling magma chamber, whereas viscoelastic and poroelastic flow from the partial melt region would cause uplift over the magma chamber and subsidence in a broad region surrounding the magma chamber. Regardless of the mechanism, these models suggest that 7–11% of the total uplift expected (and therefore magma recharge supply) during the eruptive cycle at Axial Seamount comes from shallow sources. Steady influx of magma from a deep source can explain the long-term, lower rate of uplift, and is consistent with observations from other land volcanoes.

[38] To reconstruct the uplift history at Axial, the inflation data was fit to two different uplift scenarios: (1) exponential plus linear and (2) exponential plus exponential. These model curves suggest that the volcano will fully reinflate by 2020, at which time it will be primed for another eruption. Future measurements should help distinguish between these two scenarios and refine the models of magma resupply based on the intereruption uplift history.

[39] The geodetic time series that we have been collecting at Axial Seamount is a unique data set. It is the only site in the world where active inflation is currently being measured at a submarine volcano, and it allows us to hypothesize about the length of its eruptive cycle and the physical mechanisms of magma replenishment. Continuing this unique time series will allow model and forecast testing and will further illuminate the differences and similarities between magmatic plumbing systems at submarine and subaerial volcanoes.

Acknowledgments

[40] The authors would like the thank M. Poland and C. Chadwell for constructive reviews that improved the manuscript. Our research could not have been completed

without the help of Mark Zumberge, who developed and maintains the MPR instrument package, and who has supported this project from the beginning. Special thanks to the *ROPOS* and *Jason* ROV teams who skillfully executed the MPR measurements and to the captains and crews of both the R/V *Thomas Thompson* and the R/V *Atlantis* who facilitated our scientific endeavors. The support of the NOAA/PMEL Engineering group is gratefully acknowledged. PMEL contribution number 3150. This work was funded by NOAAs West Coast and Polar Regions Undersea Research Center, the NOAA Vents Program, and the National Science Foundation (grant OCE0725605).

References

Aagaard, B., C. Williams, and M. Knepley (2007), PyLith: A finite-element code for modeling quasi-static and dynamic crustal deformation, *Eos Trans. AGU*, *88*(52), Fall Meet. Suppl., Abstract T21B-0592.

Björnsson, A. (1985), Dynamics of crustal rifting in NE Iceland, *J. Geophys. Res.*, *90*, 10,151–10,162, doi:10.1029/JB090iB12p10151.

Butterfield, D. A., R. E. McDuff, M. D. Lilley, G. J. Massoth, and J. E. Lupton (1990), Geochemistry of hydrothermal fluids from Axial Seamount Hydrothermal Emissions Study vent field, Juan de Fuca Ridge: Subseafloor boiling and subsequent fluid-rock interaction, *J. Geophys. Res.*, *95*, 12,895–12,921, doi:10.1029/JB095iB08p12895.

Chadwick, W. W., Jr., R. W. Embley, H. B. Milburn, C. Meinig, and M. Stapp (1999), Evidence for deformation associated with the 1998 eruption of Axial Volcano, Juan de Fuca Ridge, from acoustic extensometer measurements, *Geophys. Res. Lett.*, *26*, 3441–3444, doi:10.1029/1999GL900498.

Chadwick, J., M. Perfit, I. Ridley, I. Jonasson, G. Kamenov, W. Chadwick, R. Embley, P. le Roux, and M. Smith (2005), Magmatic effects of the Cobb Hotspot on the Juan de Fuca Ridge, *J. Geophys. Res.*, *110*, B03101, doi:10.1029/2003JB002767.

Chadwick, W. W., Jr., D. J. Geist, S. Jónsson, M. Poland, D. J. Johnson, and C. M. Meertens (2006a), A volcano bursting at the seams: Inflation, faulting, and eruption at Sierra Negra Volcano, Galápagos, *Geology*, *34*, 1025–1028, doi:10.1130/G22826A.1.

Chadwick, W. W., Jr., S. L. Nooner, M. A. Zumberge, R. W. Embley, and C. G. Fox (2006b), Vertical deformation monitoring at Axial Seamount since its 1998 eruption using deep-sea pressure sensors, *J. Volcanol. Geotherm. Res.*, *150*, 313–327, doi:10.1016/j.jvolgeores.2005.07.006.

Dragoni, M., and C. Magnanensi (1989), Displacement and stress produced by a pressurized, spherical magma chamber, surrounded by a viscoelastic shell, *Phys. Earth Planet. Inter.*, *56*, 316–328, doi:10.1016/0031-9201(89)90166-0.

Dvorak, J. J., and D. Dzurisin (1997), Volcano geodesy: The search for magma reservoirs and the formation of eruptive vents, *Rev. Geophys.*, *35*, 343–384, doi:10.1029/97RG00070.

Dvorak, J. J., and A. T. Okamura (1987), A hydraulic model to explain variations in summit tilt rate at Kilauea and Mauna Loa volcanoes, edited by R. W. Decker et al., in *Volcanism in Hawaii*, *U.S. Geol. Surv. Prof. Pap.*, *1350*, 1281–1296.

Dziak, R. P., and C. G. Fox (1999a), Long-term seismicity and ground deformation at Axial Volcano, Juan de Fuca Ridge, *Geophys. Res. Lett.*, *26*, 3641–3644, doi:10.1029/1999GL002326.

Dziak, R. P., and C. G. Fox (1999b), The January 1998 earthquake swarm at Axial Volcano, Juan de Fuca Ridge: Hydroacoustic evidence of seafloor volcanic activity, *Geophys. Res. Lett.*, *26*, 3429–3432, doi:10.1029/1999GL002332.

Ebinger, C. J., D. Keir, A. Ayele, E. Calais, T. J. Wright, M. Belachew, J. O. S. Hammond, E. Campbell, and W. R. Buck (2008), Capturing magma intrusion and faulting processes during continental rupture: Seismicity of the Dabbahu (Afar) rift, *Geophys. J. Int.*, *174*, 1138–1152.

Embley, R. W., and E. T. Baker (1999), Interdisciplinary group explores seafloor eruption with remotely operated vehicle, *Eos Trans. AGU*, *80*(19), 213, doi:10.1029/99EO00157.

Embley, R. W., W. W. Chadwick Jr., D. Clague, and D. Stakes (1999), The 1998 Eruption of Axial Volcano: Multibeam anomalies and seafloor observations, *Geophys. Res. Lett.*, *26*, 3425–3428, doi:10.1029/1999GL002328.

Foulger, G. R., C.-H. Jahn, G. Seeber, P. Einarsson, B. R. Julian, and K. Heki (1992), Post-rifting stress relaxation at the divergent plate boundary in northeast Iceland, *Nature*, *358*, 488–490, doi:10.1038/358488a0.

Fox, C. G. (1999), In situ ground deformation measurements from the summit of Axial Volcano during the 1998 volcanic episode, *Geophys. Res. Lett.*, *26*, 3437–3440, doi:10.1029/1999GL900491.

Fox, C. G., W. W. Chadwick Jr., and R. W. Embley (2001), Direct observation of a submarine volcanic eruption from a sea-floor instrument caught in a lava flow, *Nature*, *412*, 727–729, doi:10.1038/35089066.

Geist, D. J., K. S. Harpp, T. R. Naumann, M. Poland, W. W. Chadwick, Jr., M. Hall, and E. Rader (2008), The 2005 eruption of Sierra Negra volcano, Galapagos, Ecuador, *Bull. Volcanol.*, *70*, 655–673.

Hodge, D. S. (1974), Thermal model for origin of granitic batholiths, *Nature*, *251*, 297–299, doi:10.1038/251297a0.

Hurwitz, S., L. B. Christiansen, and P. A. Hsieh (2007), Hydrothermal fluid flow and deformation in large calderas: Inferences from numerical simulations, *J. Geophys. Res.*, *112*, B02206, doi:10.1029/2006JB004689.

Kent, G., A. Harding, J. Babcock, J. A. Orcutt, R. S. Detrick, J. P. Canales, E. M. Van Ark, S. M. Carbotte, J. Diebold, and M. Nedimovic (2003), A new view of 3-D magma chamber structure beneath Axial Seamount and Coaxial segment: Preliminary results from the 2002 multichannel seismic survey of the Juan de Fuca Ridge, *Eos Trans. AGU*, *84*(46), Fall Meet. Suppl., Abstract B12A-0755.

Lu, Z., T. Masterlark, D. Dzurisin, R. Rykhus, and C. Wicks Jr. (2003), Magma supply dynamics at Westdahl volcano, Alaska, modeled from satellite radar interferometry, *J. Geophys. Res.*, *108*(B7), 2354, doi:10.1029/2002JB002311.

Masterlark, T., and Z. Lu (2004), Transient volcano deformation sources imaged with interferometric synthetic aperture radar: Application to Seguam Island, Alaska, *J. Geophys. Res.*, *109*, B01401, doi:10.1029/2003JB002568.

Mogi, K. (1958), Relations between the eruptions of various volcanoes and the deformation of the ground surfaces around them, *Bull. Earthquake Res. Inst. Univ. Tokyo*, *36*, 99–134.

Newman, A. V., T. H. Dixon, G. I. Ofoegbu, and J. E. Dixon (2001), Geodetic and seismic constraints on recent activity at Long Valley Caldera, California: Evidence for viscoelastic rheology, *J. Volcanol. Geotherm. Res.*, *105*, 183–206, doi:10.1016/S0377-0273(00)00255-9.

Nooner, S. L. (2005), Gravity changes associated with underground injection of CO_2 at the Sleipner storage reservoir in the North Sea, and other marine geodetic studies, Ph.D. thesis, 188 pp., Univ. of California, San Diego, La Jolla, Calif.

Perfit, M. R., and W. W. Chadwick (1998), Magmatism at mid-ocean ridges: Constraints from volcanological and geochemical investigations, in *Faulting and Magmatism at Mid-Ocean Ridges*, *Geophys. Monogr. Ser.*, vol. 106, edited by W. R. Buck et al., 59–115, AGU, Washington, D.C.

Rubin, A. M. (1998), Dike ascent in partially molten rock, *J. Geophys. Res.*, *103*, 20,901–20,919, doi:10.1029/98JB01349.

Ruiz, A., D. Geist, and W. W. Chadwick Jr. (2007), Inflation of Sierra Negra Volcano since the 2005 eruption, *Eos Trans. AGU*, *87*(52), Fall Meet. Suppl., Abstract V53C-1422.

Sigmundsson, F. (2007), Deep crustal storage of large volume of magma prior to catastrophic eruptions: The role of visco-elastic response to magma accumulation, *Eos Trans. AGU*, *88*(52), Fall Meet. Suppl., Abstract V52B-02.

Sohn, R. A., A. H. Barclay, and S. C. Webb (2004), Microearthquake patterns following the 1998 eruption of Axial Volcano, Juan de Fuca Ridge: Mechanical relaxation and thermal strain, *J. Geophys. Res.*, *109*, B01101, doi:10.1029/2003JB002499.

Stenvold, T., O. Eiken, M. A. Zumberge, G. S. Sasagawa, and S. L. Nooner (2006), High-precision relative depth and subsidence mapping from seafloor water-pressure measurements, *SPE J.*, *11*, 380–389, doi:10.2118/97752-PA.

Sinton, J. M., and R. S. Detrick (1992), Mid-ocean ridge magma chambers, *J. Geophys. Res.*, *97*, 197–216, doi:10.1029/91JB02508.

Sturkell, E., P. Einarsson, F. Sigmundsson, S. Hreinsdottir, and H. Geirsson (2003), Deformation of Grimsvotn volcano, Iceland: 1998 eruption and subsequent inflation, *Geophys. Res. Lett.*, *30*(4), 1182, doi:10.1029/2002GL016460.

Sturkell, E., P. Einarsson, F. Sigmundsson, H. Geirsson, H. Olafsson, R. Pedersen, E. de Zeeuw-van Dalfsen, A. T. Linde, S. I. Sacks, and R. Stefansson (2006), Volcano geodesy and magma dynamics in Iceland, *J. Volcanol. Geotherm. Res.*, *150*, 14–34, doi:10.1016/j.jvolgeores.2005.07.010.

Tilling, R. I., and J. J. Dvorak (1993), Anatomy of a basaltic volcano, *Nature*, *363*, 125–133, doi:10.1038/363125a0.

Toomey, D. R., G. M. Purdy, S. C. Solomon, and W. S. D. Wilcock (1990), The three-dimensional seismic velocity structure of the East Pacific Rise near latitude 9°30′N, *Nature*, *347*, 639–645, doi:10.1038/347639a0.

Tryggvason, E. (1980), Subsidence events in the Krafla area, North Iceland, 1975–1979, *J. Geophys.*, *47*, 141–153.

Tryggvason, E. (1994), Surface deformation at the Krafla volcano, North Iceland, 1982–1992, *Bull. Volcanol.*, *56*, 98–107.

Van Heeswijk, M. (1986), *Shallow Crustal Structure of the Caldera of Axial Seamount, Juan de Fuca Ridge*, Oreg. State Univ., Corvallis.

Vera, E. E., J. C. Mutter, P. Buhl, J. A. Orcutt, A. J. Harding, M. E. Kappus, R. S. Detrick, and T. M. Brocher (1990), The structure of 0- to 0.2-m.y.-old oceanic crust at 9°N on the East Pacific Rise from expanded spread profiles, *J. Geophys. Res.*, *95*, 15,529–15,556, doi:10.1029/JB095iB10p15529.

West, M. E., W. Menke, M. Tolstoy, S. Webb, and R. Sohn (2001), Magma storage beneath Axial Volcano on the Juan de Fuca mid-ocean ridge, *Nature*, *413*, 833–836, doi:10.1038/35101581.

West, M., W. Menke, and M. Tolstoy (2003), Focused magma supply at the intersection of the Cobb hotspot and the Juan de Fuca ridge, *Geophys. Res. Lett.*, *30*(14), 1724, doi:10.1029/2003GL017104.

Wilcock, W. S. D., S. C. Solomon, G. M. Purdy, and D. R. Toomey (1992), The seismic attenuation structure of a fast-spreading mid-ocean ridge, *Science*, *258*, 1470–1474, doi:10.1126/science.258.5087.1470.

Williams, C. A. (2006), Development of a package for modeling stress in the lithosphere, *Eos Trans. AGU*, *87*(36), Jt. Assem. Suppl., Abstract T24A-01.

Williams, C. A., B. Aagaard, and M. G. Knepley (2005), Development of software for studying earthquakes across multiple spatial and temporal scales by coupling quasi-static and dynamic simulations, *Eos Trans. AGU*, *86*(52), Fall Meet. Suppl., Abstract S53A-1072.

Wright, T. J., C. Ebinger, J. Biggs, A. Ayele, G. Yirgu, D. Keir, and A. Stork (2006), Magma-maintained rift segmentation at continental rupture in the 2005 Afar dyking episode, *Nature*, *442*, 291–294, doi:10.1038/nature04978.